Experimental approach for IR-UWB Radar-Based people detection in Industry 4.0 environments

Zaynab Baydoun, Roua Youssef, Emanuel Radoi, Stéphane Azou, Tina Yaacoub, David Espes

Experimental approach for IR-UWB Radar-Based people detection in Industry 4.0 environments

Zaynab BAYDOUN
Univ Brest, CNRS, Lab-STICC
Brest, France
Email: zaynab.baydoun@univ-brest.fr

Roua YOUSSEF
Univ Brest, CNRS, Lab-STICC
Brest, France
Email: roua.youssef@univ-brest.fr

Emanuel RADOI
Univ Brest, CNRS, Lab-STICC
Brest, France
Email: emanuel.radoi@univ-brest.fr

Stéphane AZOU
ENIB, CNRS, Lab-STICC
Plouzané, France
Email: azou@enib.fr

Tina YAACOUB
Saint Joseph University
Beyrouth, Lebanon
Email: tina.yaacoub@usj.edu.lb

David ESPES
Univ Brest, CNRS, Lab-STICC
Brest, France
Email: david.espes@univ-brest.fr

***Abstract*—An experimental investigation of people detection in Industry 4.0 environments, using impulse radio ultra-wideband signals, is described in this paper. Given the specific characteristics of the considered indoor environment and signals of interest, we first address clutter reduction, and then propose a two-paths signal processing architecture for constant false alarm rate (CFAR) detection of moving and stationary people, using matched filtering and Doppler focusing, respectively. A statistical study of the residual clutter and noise is carried out, and optimal threshold values are derived for these two use cases. The performance of the two CFAR detectors is then assessed using simulated data for different signal-to-noise ratios (SNR) and false alarm probabilities. Finally, their detection capabilities are explored using real data, measured in a heavily cluttered Industry 4.0 indoor environment, for a specially designed scenario with a person alternating between stop and motion phases.**

***Index Terms*—Impulse Radio Ultra-Wideband, Indoor people detection, Industry 4.0 environment, CFAR detection.**

I. Introduction

In today's increasingly automated world, the importance of effective human-machine interaction cannot be overstated. With applications spanning military operations, safety protocols, security measures, and entertainment endeavors, the transition from manual to automated machinery and robotics requires a seamless collaboration between humans and machines [1]. An essential aspect of this collaboration lies in ensuring the safety and efficiency of human presence alongside autonomous systems.

Among multiple techniques, recent years have witnessed remarkable strides in Impulse Radio Ultra-Wideband (IR-UWB) technology [2], particularly in its application to human detection scenarios. Moreover, it is utilized in various fields, including military, automotive, radar imaging for medicine [3], complex situation [4], security systems for intrusion detection and surveillance [5], and other security purposes, due to its material penetrating capability [6] [7]. These IR-UWB sensors transmit short radio pulses typically spanning between 3.1 and 10.6 GHz, enabling high-resolution detection and measurement capabilities.

People detection and tracking using IR-UWB technology involves assessing spatio-temporal properties including their presence, counting, localization and identification. This technology distinguishes various human characteristics, enabling detection of the human body and its movements, from fast or slow walking paces to small motions of hands and feet, and even vital signs such as heartbeats and breathing [8]–[10].

IR-UWB sensors can be successfully used for human detection scenarios, whether in line-of-sight (LOS) conditions or even in challenging conditions like through-wall detection and dense environments. In this case, additional algorithms are necessary for clutter removal, including Singular Value Decomposition (SVD), Kalman filter, exponential averaging algorithm, adaptive clutter reduction, and Moving Target Indicator (MTI) [11]–[15].

Our original contribution in this paper is threefold. We first propose a two-paths CFAR detection scheme, designed to detect moving and static people using a single snapshot and multiple snapshots, respectively. Another important contribution is the study of the statistical distribution of the residual clutter and noise after clutter reduction at the output of the matched filter (MF) and Doppler focusing (DF) respectively, and the evaluation of the CFAR detectors performance using simulated data. While the identification of the Rayleigh distribution as the best match in the first case is straightforward, our finding related to the best fitted Nakagami distribution in the second case can be considered as an original result. Finally, our third contribution is to demonstrate the effectiveness of the proposed detection approach using measured data, in a realistic smart factory-like environment.

The remainder of the paper is organized as follows. Section II introduces the system model and explains the various steps of UWB signal processing. Section III deals with the statistical analysis of residual clutter and noise and provides detection performance curves obtained by simulation. Section IV describes the experimental setup and shows the results obtained for both moving and stationary people detection, using data measured in a Industry 4.0 indoor environment.

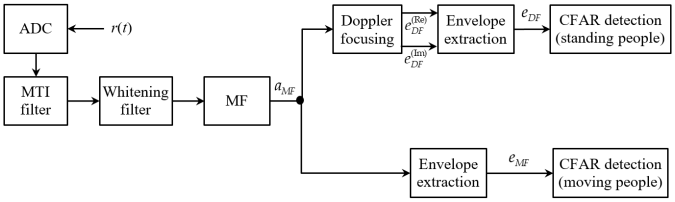

Fig. 1: UWB signal processing flowchart for people detection

Finally, some concluding remarks are drawn and future work is planned in Section V.

II. System model

The proposed UWB signal processing flowchart is shown in Fig. 1. The system model includes several signal processing stages, including MTI, whitening filter, MF and DF. The noiseless signal received by the IR-UWB sensor during one pulse repetition interval (PRI) can be written as:

$$r_n(t) = \sum_{l=1}^{L} \sigma_l^{(n)} p(t - \tau_l^{(n)} - nT_r) e^{-j2\pi f_l^{(n)} nT_r}, \quad t \in [nT_r, (n+1)T_r] \tag{1}$$

where L represents the number of resolvable scattering points, each at a range resolution of $\delta R = c/(2B)$, c denotes the speed of electromagnetic waves, and B stands for the bandwidth of the T_r-periodically transmitted UWB waveform $p(t)$. As well, we have the associated reflectivities σ_l, delays $\tau_l = (2R_l)/c$ for $l = 1, \ldots, L$, and Doppler shifts f_l.

To mitigate the indoor environment clutter, a first-order MTI filter [15] subtracts signals between consecutive PRIs, which eliminates reflections from stationary objects, as their delays and reflectivity remain constant, resulting in null Doppler shifts. Since the low Doppler frequencies associated with human breathing are also considerably weakened, a whitening filter is used to compensate for the MTI effect and thus enable the detection of stationary people.

One notable difference from conventional radar processing is how targets are managed during the coherent integration time (CIT) associated with Doppler focusing. In standard narrowband radar systems, targets typically persist within the same range resolution cell during this CIT. However, in our system, the wide bandwidth of the transmitted signal results in a very fine slant range resolution, typically around 10 cm. Consequently, the DF hypothesis does not hold anymore for moving people, so that their CFAR detection has to be done directly at the MF output. For stationary people, CFAR detection follows DF, leveraging their breathing-associated Doppler frequency (approximately 0.4 Hz). Additionally, Doppler patterns from walking individuals aid in distinguishing targets.

To accurately find out the optimal CFAR detection threshold, a statistical study of the residual clutter plus noise (RCN) is carried out in the next section, at the output of the MF and DF stages, for moving and stationary people detection, respectively.

III. Statistical analysis

In the context of heavy-cluttered environments, like Industry 4.0 [16], the detection of signal of interest (SoI) is challenging due to the abundance of resolvable signals backscattered by the other objects from the environment. The statistical study and the detection performance curves provided in this section are performed considering an IEEE 802.15.4a CM7 model [17], which is well suited to such an indoor environment.

We first note that for the signal processing flow chart represented in Fig. 1, the MF is basically a linear and time-invariant (LTI) pass-band filter, while the RCN at its input can be considered as a real centered AWGN. Hence, according to [18], the noise amplitude a_{MF} and the noise envelope e_{MF} at the MF output, follow normal and Rayleigh distributions, respectively. Therefore, $a_{MF} \sim N(0, \sigma^2)$, while the expression of the Rayleigh distribution corresponding to e_{MF} is given by:

$$p_{MF_{out}}(e_{MF}; \sigma) = \frac{e_{MF}}{\sigma} \exp\left(-\frac{e_{MF}^2}{2\sigma^2}\right) \tag{2}$$

where σ is both the Rayleigh distribution parameter and the standard deviation of the normal distribution associated to a_{MF}. This parameter can be estimated by averaging the values of e_{MF} inside a N_{win}-length sliding window, using (3), where E stands for the mathematical expectation:

$$\sigma = \sqrt{\frac{2}{\pi}} E(e_{MF}) \Rightarrow \hat{\sigma} = \sqrt{\frac{2}{\pi}} \sum_{n=1}^{N_{win}} e_{MF}(n) \tag{3}$$

As shown in Fig. 2(a), $p_{MF_{out}}(e_{MF}; \hat{\sigma})$ fits well the distribution of RCN envelope at the MF output, this hypothesis is further validated by both chi-square and Kolmogorov-Smirnov tests, with a significance level of 0.05.

For stationary people detection, the real and imaginary parts of the DF output remain normally distributed after the N_{fft}-points slow time FFT, with the variance $\sigma_{DF}^2 = N_{fft}\sigma^2$, so that $Re\{a_{DF}\} \sim N(0, N_{fft}\sigma^2)$ and $Im\{a_{DF}\} \sim N(0, N_{fft}\sigma^2)$. In this case, according to the result mentioned above, their envelopes, denoted by $e_{DF}^{(\mathrm{Re})}$ and $e_{DF}^{(\mathrm{Im})}$, will be Rayleigh distributed, with the parameter $\sqrt{N_{fft}}\sigma$. We propose to consider the following detection statistic for the stationary people CFAR detection:

$$e_{DF} = \sqrt{\left(e_{DF}^{(\mathrm{Re})}\right)^2 + \left(e_{DF}^{(\mathrm{Im})}\right)^2} \tag{4}$$

According to [19], the two terms $\left(e_{DF}^{(\mathrm{Re})}\right)^2$ and $\left(e_{DF}^{(\mathrm{Im})}\right)^2$ are then exponentially distributed with the parameter $\lambda = 1/\left(2N_{fft}\sigma^2\right)$ and their sum $\left(e_{DF}^{(\mathrm{Re})}\right)^2 + \left(e_{DF}^{(\mathrm{Im})}\right)^2$ follows a Gamma distribution with the shape parameter $a = 2$ and the scale parameter $b = 2N_{fft}\sigma^2$. Still according to [19], we can finally conclude that e_{DF} follows the Nakagami distribution with the same shape parameter ($a = 2$) and the scale parameter $\Omega = 2b = 4N_{fft}\sigma^2$, given by:

$$p_{DF_{out}}(e_{DF}; 2, \Omega) = \frac{8}{\Omega^2} e_{DF}^3 \exp\left(-\frac{2}{\Omega} e_{DF}^2\right) \tag{5}$$

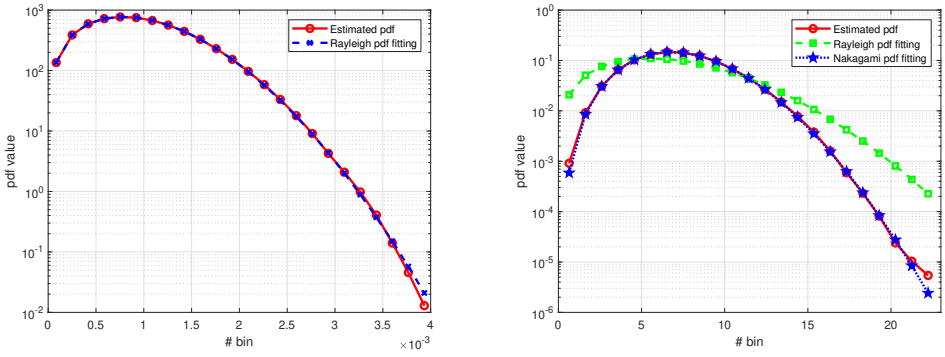

(a) (b)

Fig. 2: Estimated pdf fitting for the envelope of RCN at the: (a) MF output and (b) DF output

The scale parameter Ω can be also estimated using a N_{win}-length sliding window, but by averaging the square values of e_{DF} inside the window, as shown by the equation below:

$$\Omega = E\left(e_{DF}^2\right) \Rightarrow \hat{\Omega} = \sum_{n=1}^{N_{win}} e_{DF}^2(n) \tag{6}$$

Just as for the MF output statistical analysis, our finding is confirmed by Fig. 2(b), which shows the good match between $p_{DF_{out}}\left(e_{DF}; 2, \hat{\Omega}\right)$ and the RCN envelope at the DF output, this hypothesis being again further validated by the chi-square and Kolmogorov-Smirnov tests, with the same significance level. The best-fitted Rayleigh distribution is also plotted as a reference.

Since the RCN envelope distribution is completely determined at both MF and DF output, a standard CA-CFAR (Cell Averaging CFAR) scheme [20] can be used to perform people detection, with the detection thresholds provided by:

$$\begin{cases} T_{MF} = \hat{\sigma}\sqrt{2\ln\left(1/P_{fa}\right)} \\ T_{DF} = cdf_{Nakagami}^{-1}\left(1 - P_{fa}; 2, \hat{\Omega}\right) \end{cases} \tag{7}$$

where P_{fa} is the required level of constant false alarm probability and $cdf_{Nakagami}^{-1}(.)$ is the inverse of the Nakagami cumulative function.

Relying on the statistical study above, the CFAR detection performance has been evaluated using simulated data, in a scenario with one stationary and two moving people. The curves of the detection rate against the in-band SNR at the MF input are plotted in Fig. 3 for three values of the false alarm probability, in the case when the CFAR detection is performed at the MF and DF output. While the MF gain, corresponding to the product between the signal duration and its bandwidth, applies to both cases, an additional processing gain, proportional to the DF coherent integration time, also comes into play in the second case. For our Monte Carlo simulations, we have used the Novelda waveform parameters provided in Table I, and considered 4000 transmitted pulses in the multiple snapshots case, for each one of the 10^4 independent trials, which corresponds to a DF coherent integration time of 20 seconds, given the value of 200 FPS (frames per second) selected in the radar configuration.

TABLE I: Novelda Radar parameters

Parameter	Value
output power	13.6 dBm
center frequency	8.7 GHz
pulse repetition frequency	120 MHz
sampling frequency	23.3 GHz
slow time sampling frequency	30 Hz

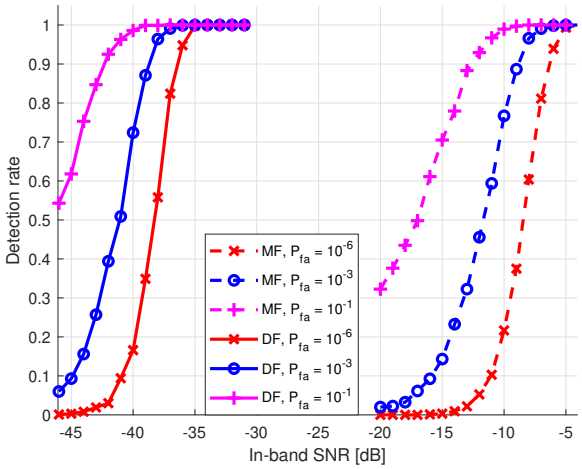

Fig. 3: CFAR detection simulation results obtained using Novelda waveform, at the MF and DF output

IV. Experimental results

The experimental approach described in this section illustrates the two processing paths for people CFAR detection in the Industry 4.0 indoor environment of the University of Brest shown in Fig. 4. It represents a drug industrial production chain, with all the associated supervision and cybersecurity infrastructure. During our experiments the platform was running, so that the Doppler spectrum generated by its mobile components and conveyors, as well as the signal backscattered by its rigid structure are mixed with the SoI, backscattered by a person present in the room.

In our experimental setup, we have used a Xethru X4M03 IR-UWB Novelda radar [21], having the parameters given in Table I. It has been connected to a laptop for data storage and

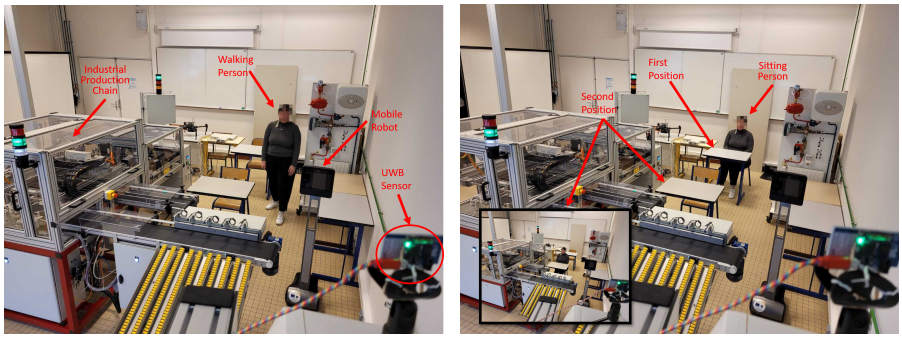

(a) (b)

Fig. 4: Experimental setup in the industrial platform used for measured data acquisition and illustration of the two main phases of the considered scenario: (a) person walking in front of the radar, and (b) person sitting

analysis, utilizing MATLAB® software for data processing. The data acquisition period spans 120 seconds, during which the person to be detected alternates between sitting and moving alongside the industrial platform. We have considered a combined scenario including 4 distinct phases: the person sits at about 5.5 m away from the radar during 50 seconds, then slowly moves back and forth in front of the radar within the range 2.5-5 m, during 20 seconds, sits again at about 4 m for 30 seconds, and finally walks faster than in the second phase during the last 20 seconds.

The signal processing results corresponding to the considered scenario are provided in Fig. 5. The envelope of the measured signals is first shown in Fig. 5(a). The backscattered signals are measured in each PRI during the fast time, their delays being directly related to the slant range represented on the vertical axis of the plotted images. The other axis is the slow time, which refers to the time required to transmit the 4000 snapshots to be used by the Doppler focusing stage. It can be readily seen from this image that the considered indoor environment is heavily-cluttered, making it difficult to detect people inside. The most part of the clutter, corresponding to fixed objects, is removed after the MTI stage, as illustrated in Fig. 5(b), but the signal corresponding to the person's stationary positions is also highly attenuated because the breathing rate is very low (around 0.4 Hz). This effect is compensated by the whitening filter, which restores the SNR corresponding to the signal backscattered by the stationary person, as shown in Fig. 5(c).

The SNR is further maximized for all the backscattered signals by the MF, as can be seen in Fig. 5(d), the associated processing gain being of about 4.5 dB. Note that MF operates in fast time, unlike the two previous signal processing steps, which are performed in slow time, just as the last processing stage, i.e. Doppler focusing. Its effect is shown in Fig. 5(e) and Fig. 5(f) for two Doppler shift ranges, under and above 1 Hz, respectively. This separation is useful since the stationary people can be detected in the first region, while the Doppler spectrum associated with the moving people and mobile parts of the industrial production chain is visible on the second region. Indeed, the person's breath during the two time intervals when she is seated can be clearly identified in Fig. 5(e), by

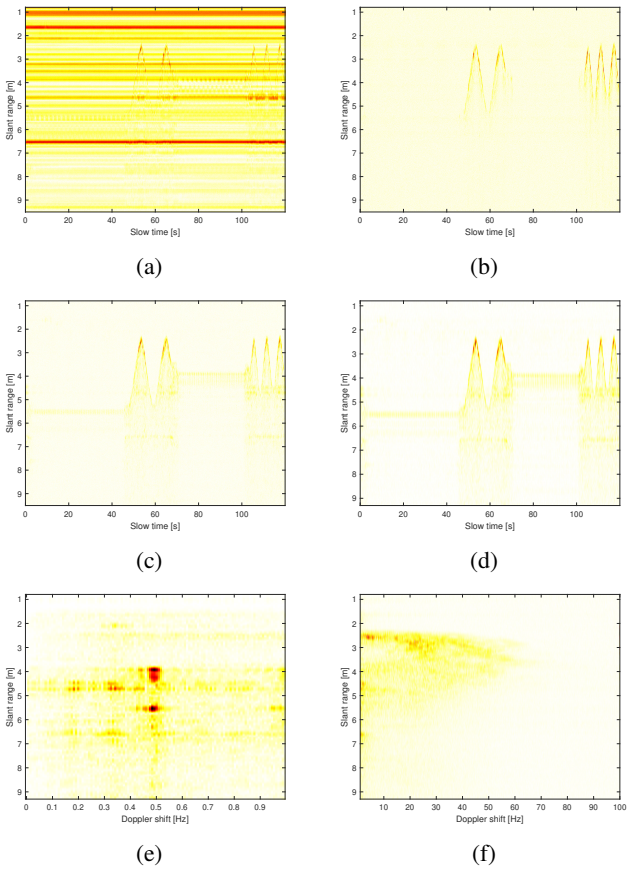

(a) (b) (c) (d) (e) (f)

Fig. 5: Signal processing results for measured data in an Industry 4.0 indoor environment: (a) measured data, (b) MTI output, (c) whitening filter output, (d) MF output, (e) DF output under 1 Hz and (b) DF output above 1 Hz

the two maxima located at 4 m and 5.5 m, corresponding to a Doppler shift of about 0.5 Hz. Their amplitudes are similar, although the second sitting position is closer than the first one, because the processing gain is higher for the first position, due to a longer coherent integration time, i.e. 50 seconds instead of 30 seconds for the second position. It also explains the better Doppler resolution, which can be noticed for the first position compared to the second one.

Finally, the CFAR detection results at the MF and DF output

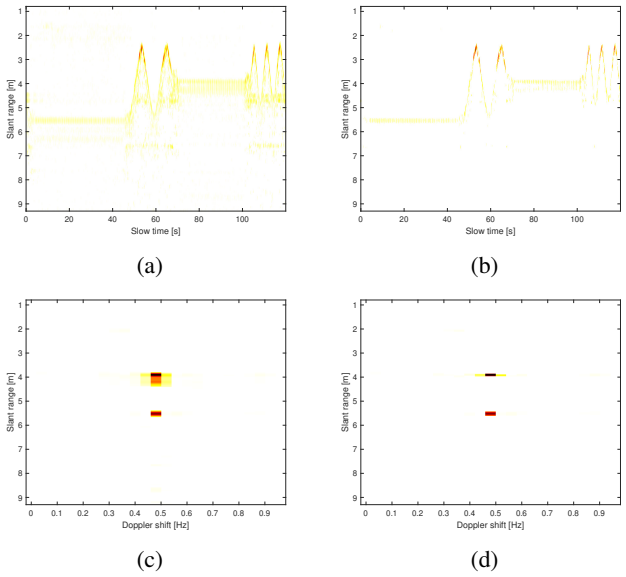

(a) (b) (c) (d)

Fig. 6: CFAR detection results for measured data in an Industry 4.0 indoor environment: (a) at the MF output ($P_{fa} = 10^{-1}$), (b) at the MF output ($P_{fa} = 10^{-6}$), (c) at the DF output ($P_{fa} = 10^{-1}$) and (d) at the DF output ($P_{fa} = 10^{-6}$)

are illustrated in Fig. 6, for two false alarm probabilities, i.e. 10^{-1} and 10^{-6}. The detection thresholds (7), derived in Section III, have been used to obtain these results, by making a decision on each MF/DF output envelope sample or decision statistic. They have been calculated by averaging 100 measured samples around the decision statistic, according to (3) and (6), with a guard interval equal to the fast time and Doppler resolution, respectively.

As it can be readily seen, the person inside the room is correctly detected, both during the motion and stillness time intervals. All four phases of the scenario under consideration are reliably recovered, so that the detection results can be further used for tracking or people identification purposes. We have also noticed an accurate estimation of the required false alarm rate for the regions where only the RCN is present.

V. Conclusion

The experimental UWB system for people detection in cluttered industrial environments has shown promising results, with effective clutter and noise mitigation performed by its signal processing stages. Our findings demonstrate a high probability of detection for both static and moving people, highlighting the system's suitability for industrial applications. Future research will focus on refining clutter mitigation algorithms and exploring machine learning integration to distinguish between the Doppler signatures of mobiles objects and people moving in indoor environment.

Acknowledgment

This research work has been partially funded by Brittany region. The authors would also like to express their gratitude to the University of Brest and Lab-STICC, CNRS, UMR 6285, for providing access to the Industry 4.0 platform.

References

[1] T. Czimmermann, M. Chiurazzi, M. Milazzo, S. Roccella, M. Barbieri, P. Dario, C. M. Oddo, and G. Ciuti, "An autonomous robotic platform for manipulation and inspection of metallic surfaces in industry 4.0," *IEEE Transactions on Automation Science and Engineering*, vol. 19, no. 3, pp. 1691–1706, 2022.

[2] M. Cheraghinia, A. Shahid, S. Luchie, G.-J. Gordebeke, O. Caytan, J. Fontaine, B. Van Herbruggen, S. Lemey, and E. De Poorter, "A comprehensive overview on uwb radar: Applications, standards, signal processing techniques, datasets, radio chips, trends and future research directions," *arXiv preprint arXiv:2402.05649*, 2024.

[3] F. Thiel, O. Kosch, and F. Seifert, "Ultra-wideband sensors for improved magnetic resonance imaging, cardiovascular monitoring and tumour diagnostics," *Sensors*, vol. 10, no. 12, pp. 10 778–10 802, 2010.

[4] Z. Li, Q. An, F. Qi, F. Liang, H. Lv, Y. Zhang, X. Yu, and J. Wang, "Detection of People Trapped under the Ruins Using Dual-frequency IR-UWB Radar," in *2018 15th European Radar Conference (EuRAD)*. Madrid: IEEE, Sep. 2018, pp. 83–86.

[5] F. Khan, S. Azou, R. Youssef, P. Morel, E. Radoi, and O. A. Dobre, "An IR-UWB multi-sensor approach for collision avoidance in indoor environments," *IEEE Transactions on Instrumentation and Measurement*, vol. 71, pp. 1–13, 2022.

[6] J. Li, Z. Zeng, J. Sun, and F. Liu, "Through-wall detection of human being's movement by UWB radar," *IEEE Geoscience and Remote Sensing Letters*, vol. 9, no. 6, pp. 1079–1083, 2012.

[7] X. Chen and W. Chen, "Multipath ghost elimination for through-wall radar imaging," *IET Radar, Sonar & Navigation*, vol. 10, no. 2, pp. 299–310, 2016. [Online]. Available: https://ietresearch.onlinelibrary.wiley.com/doi/abs/10.1049/iet-rsn.2015.0171

[8] T. Pan, Y. Guo, W. Guo, and C. Kang, "Detection of vital sign based on uwb radar by a time domain coherent accumulation method," *IEEE Sensors Journal*, vol. 23, no. 15, pp. 17 054–17 063, 2023.

[9] X. Dang, J. Zhang, and Z. Hao, "A non-contact detection method for multi-person vital signs based on ir-uwb radar," *Sensors*, vol. 22, no. 16, 2022.

[10] J. Park and S. H. Cho, "IR-UWB radar sensor for human gesture recognition by using machine learning," in *2016 IEEE 18th International Conference on High Performance Computing and Communications*, 2016, pp. 1246–1249.

[11] F. H. C. Tivive and A. Bouzerdoum, "An improved SVD-based wall clutter mitigation method for through-the-wall radar imaging," in *2013 IEEE 14th Workshop on Signal Processing Advances in Wireless Communications (SPAWC)*, 2013, pp. 430–434.

[12] H. Yan, R. Wang, C. Gao, Y. Deng, and M. Zheng, "A novel clutter suppression algorithm with Kalman filtering," in *2013 IEEE Radar Conference (RadarCon13)*. IEEE, 2013.

[13] V.-H. Nguyen and J.-Y. Pyun, "Location detection and tracking of moving targets by a 2D IR-UWB radar system," *Sensors*, 2015.

[14] S. Yoo, S. Chung, D.-M. Seol, and S. H. Cho, "Adaptive clutter suppression algorithm for detection and positioning using IR-UWB radar," in *2018 9th International Conference on Ultrawideband and Ultrashort Impulse Signals (UWBUSIS)*, 2018, pp. 40–43.

[15] M. Skolnik, *Radar Handbook, Third Edition*, ser. Electronics electrical engineering. McGraw-Hill Education, 2008. [Online]. Available: https://books.google.fr/books?id=76uF2Xebm-gC

[16] X. Li, D. Li, J. Wan, A. Vasilakos, C.-F. Lai, and S. Wang, "A review of industrial wireless networks in the context of industry 4.0," *Wireless Networks*, vol. 23, 01 2017.

[17] A. F. Molisch, "Ultra-Wide-Band Propagation Channels," *Proceedings of the IEEE*, vol. 97, no. 2, pp. 353–371, Feb. 2009.

[18] J. Proakis and M. Salehi, *Communication Systems Engineering*, ser. Pearson Education. Prentice Hall, 2002. [Online]. Available: https://books.google.fr/books?id=8WqfQgAACAAJ

[19] J. Gubner and a. O. M. C. Safari, *Probability and Random Processes for Electrical and Computer Engineers*, ser. EngineeringPro collection. Cambridge University Press, 2006. [Online]. Available: https://books.google.fr/books?id=xs2vDAEACAAJ

[20] B. Mahafza, *Radar Systems Analysis and Design Using MATLAB*. CRC Press, 2022. [Online]. Available: https://books.google.fr/books?id=CrZZEAAAQBAJ

[21] X4 - Datasheet by Novelda, "X4m03 datasheet," Novelda, Tech. Rep., 2017. [Online]. Available: https://novelda.com/wp-content/uploads/2023/03/x4_datasheet_RevA.pdf